UDK 539.4

Evaluation of the Elastic-Plastic Mixity Parameters on the Base of Different Crack Propagation Criteria. Part 2. Solution and Results

V. N. Shlyannikov and Zh. M. Sakhabutdinov

Kazan State Power Engineering University, Kazan, Russia

УДК 539.4

Оценка упругопластического параметра смешанности на основе различных критериев роста трещины. Сообщение 2. Метод решения и результаты

В. Н. Шлянников, Ж. М. Сахабутдинов

Казанский государственный энергетический университет, Казань, Россия

Предложен новый подход к решению задач смешанных видов разрушения, основанный на деформационной теории пластичности со степенным упрочнением и на использовании упругого и пластического параметров смешанности. В зависимости от условий смешанности нагружения и исходного направления линии трещины этот подход позволяет оценить широкий спектр возможных траекторий распространения трещины: по механизмам сдвига и отрыва. Для двухмерной задачи в полярной системе координат используется уравнение равновесия с функцией Эри. Для материала со степенным упрочнением применяется модель Рамберга–Осгуда. С помощью метода конечных разностей получено численное решение задачи смешанного нагружения для граничных условий, соответствующих двум случаям распространения трещины. На основании предложенного подхода оценены зависимости параметров смешанности от различных параметров нагружения и наклона трещины при разных значениях показателя упрочнения, которые хорошо согласуются с экспериментальными данными.

Ключевые слова: поведение трещин при смешанном типе деформирования, маломасштабная текучесть, смена механизма разрушения, рост трещины, параметры смешанности.

Governing Equations. In this section, we will follow the development of the governing equations of crack-tip fields for strain-hardening material. We will then use these equations to construct mixed-mode crack-tip fields for two crack growth direction criteria or competing fracture mechanisms under both plane strain and plane stress conditions. We consider a crack with the crack front parallel to the z-axis in the Cartesian coordinate system, x, y, and z, where the z-axis is perpendicular to the $x-y$ plane. Let r and θ denote the polar coordinates centered at the crack tip, while β is the angle of crack plane orientation with respect to the y-axis (Fig. 1).

Within the context of small strain approach, the equilibrium equations are

$$\frac{\partial \sigma_{rr}}{\partial r} + \frac{1}{r}\frac{\partial \sigma_{r\theta}}{\partial \theta} + \frac{\sigma_{rr} - \sigma_{\theta\theta}}{r} = 0, \qquad (1a)$$

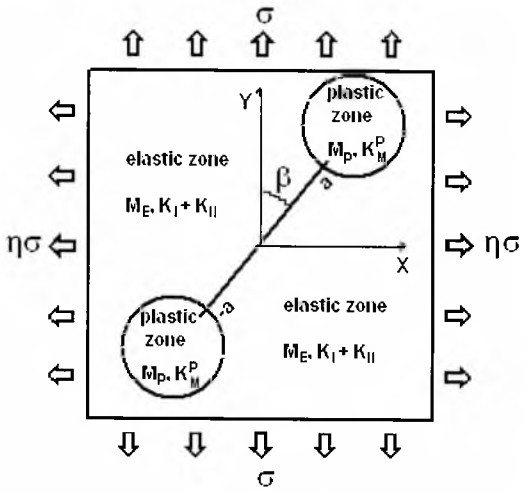

Fig. 1. The biaxially loaded inclined crack and the near and far fields.

$$\frac{1}{r}\frac{\partial \sigma_{\theta\theta}}{\partial \theta} + \frac{\partial \sigma_{r\theta}}{\partial r} + \frac{2}{r}\sigma_{r\theta} = 0. \tag{1b}$$

For two-dimensional plane problems, equilibrium is ensured for all stresses derived from the Airy stress function by

$$\sigma_{rr} = \frac{1}{r}\frac{\partial \phi}{\partial r} + \frac{1}{r^2}\frac{\partial^2 \phi}{\partial \theta^2}, \qquad \sigma_{\theta\theta} = \frac{\partial^2 \phi}{\partial r^2}, \qquad \sigma_{r\theta} = -\frac{\partial}{\partial r}\left(\frac{1}{r}\frac{\partial \phi}{\partial \theta}\right). \tag{2}$$

The partial differential equation governing the Airy stress function (2) (under the restriction of no unloading) can be obtained by eliminating the strains from the compatibility equation

$$\frac{1}{r}\frac{\partial^2 (r\varepsilon_{\theta\theta})}{\partial r^2} + \frac{1}{r^2}\frac{\partial^2 \varepsilon_{rr}}{\partial \theta^2} - \frac{1}{r}\frac{\partial \varepsilon_{rr}}{\partial r} - \frac{2}{r^2}\frac{\partial}{\partial r}\left(r\frac{\partial \varepsilon_{r\theta}}{\partial \theta}\right) = 0. \tag{3}$$

The material is assumed to obey the total deformation theory of plasticity with a power-law hardening stress-strain response. Plastic deformation is assumed to be independent of the hydrostatic component of the stress, $p = \sigma_{kk}/3$, and, further, is assumed to be completely determined by the first invariant of the stress deviator

$$s_{ij} = \sigma_{ij} - \frac{1}{3}\sigma_{kk}\delta_{ij}. \tag{4}$$

The generalized stress-strain relation is

$$E\varepsilon_{ij} = (1+\nu)s_{ij} + \frac{1-2\nu}{3}\sigma_{kk}\delta_{ij} + \frac{3}{2}\alpha_0 \sigma_e^{n-1} s_{ij}, \tag{5}$$

where ν is Poisson's ratio and σ_e is the effective stress defined by $\sigma_e^2 = \frac{3}{2} s_{ij} s_{ij}$. In simple tension, constitutive equation (5) for strain-hardening material reduces to the model suggested by Ramberg and Osgood

$$\varepsilon = \begin{cases} \sigma/E, & \sigma \le \sigma_0, \\ \sigma/E + \alpha_0 (\sigma/E)^n, & \sigma > \sigma_0. \end{cases} \tag{6}$$

In the above relation, α_0 and n are the hardening parameters, while σ_0 is the yield stress in simple tension. The yield condition for strain-hardening material can be assumed to have the form $\sigma_e = \sigma_0$ or $\sigma_e/\sigma_0 = 1$.

The dominant singularity solution for a cracked plate of a strain-hardening material, known as the HRR-singular field [1, 2]), was completed by the solution for the mixed-mode elastic-plastic stress distribution, corresponding only to tensile fracture mechanism, presented by Shih [3]. According to these approaches, the dominant singularity governing the asymptotic behavior of the stresses at the crack tip has the following form:

$$\begin{aligned} \sigma_{ij} &= \sigma_0 K_M^p r^{-1/(n+1)} \tilde{\sigma}_{ij}, \\ \sigma_e &= \sigma_0 K_M^p r^{-1/(n+1)} \tilde{\sigma}_e, \end{aligned} \tag{7}$$

where K_M^p is the plastic stress intensity factor, and M_P is the near-field mixity parameter of Shih [3]. The dimensionless functions $\tilde{\sigma}_{ij}$ and $\tilde{\sigma}_e$ depend only on the polar angle θ, M_P, and n. Under plane strain conditions, when the elastic strains are negligible and the dimensionless effective stress is related to both the stress components and the Airy dimensionless stress function $\tilde{\phi}$, the following expression holds:

$$\tilde{\sigma}_e^2 = \frac{3}{4} (\tilde{\sigma}_{rr} - \tilde{\sigma}_{\theta\theta})^2 + 3\tilde{\sigma}_{r\theta}^2, \tag{8}$$

whereas the relationship under plane stress conditions is given by:

$$\tilde{\sigma}_e^2 = \tilde{\sigma}_{rr}^2 + \tilde{\sigma}_{\theta\theta}^2 - \tilde{\sigma}_{rr}\tilde{\sigma}_{\theta\theta} + 3\tilde{\sigma}_{r\theta}^2, \tag{9}$$

where

$$\tilde{\sigma}_{rr} = s\tilde{\phi} + \frac{\partial^2 \tilde{\phi}}{\partial \theta^2}, \qquad \tilde{\sigma}_{\theta\theta} = s(s-1)\tilde{\phi}, \qquad \tilde{\sigma}_{r\theta} = (1-s)\frac{\partial \tilde{\phi}}{\partial \theta}.$$

In the present work, the fourth-order differential equation governing the dominant singularity derived from the compatibility equation is expressed in the form of an eigenvalue equation for s, by taking into account Eqs. (8) and (9). For plane strain, we get

$$\left(\frac{d^2}{d\theta^2} - a_1\right)\left[\tilde{\sigma}_e^{n-1}\left(a_2\tilde{\phi} + \frac{d^2\tilde{\phi}}{d\theta^2}\right)\right] + a_3 \frac{d}{d\theta}\left(\tilde{\sigma}_e^{n-1}\frac{d\tilde{\phi}}{d\theta}\right) = 0, \tag{10}$$

where

$$\tilde{\sigma}_e^2 = \frac{3}{4}\left(a_2\tilde{\phi} + \frac{d^2\tilde{\phi}}{d\theta^2}\right)^2 + a_4\left(\frac{d\tilde{\phi}}{d\theta}\right)^2,$$

$$a_1 = n(s-2)[n(s-2)+2], \qquad a_2 = s(2-s),$$

$$a_3 = 4(s-1)[n(s-2)+1], \qquad a_4 = 3(1-s)^2,$$

while the differential equation for plane stress is given by:

$$\left[n(s-2) - \frac{d^2}{d\theta^2}\right]\left[\tilde{\sigma}_e^{n-1}\left(s(s-3)\tilde{\phi} - 2\frac{d^2\tilde{\phi}}{d\theta^2}\right)\right] +$$

$$+ n(s-2)[n(s-2)+1]\tilde{\sigma}_e^{n-1}\left[s(2s-3)\tilde{\phi} - \frac{d^2\tilde{\phi}}{d\theta^2}\right] +$$

$$+ 6(s-1)[n(s-2)+1]\frac{d}{d\theta}\left(\tilde{\sigma}_e^{n-1}\frac{d\tilde{\phi}}{d\theta}\right) = 0, \tag{11}$$

where

$$\tilde{\sigma}_e^2 = s^2(s^2 - 3s + 3)\tilde{\phi}^2 + 3(s-1)^2\tilde{\phi}_1^2 + \tilde{\phi}_2^2 + s(3-s)\tilde{\phi}\tilde{\phi}_2.$$

Boundary Conditions. For a stress-free crack, boundary conditions on both upper and lower crack lips can be taken as

$$\begin{aligned} &\tilde{\sigma}_{\theta\theta}(-\pi) = 0, \quad \tilde{\sigma}_{r\theta}(-\pi) = 0, \quad \text{or} \quad \tilde{\phi}(-\pi) = 0, \quad \tilde{\phi}_1(-\pi) = 0, \\ &\tilde{\sigma}_{\theta\theta}(\pi) = 0, \quad \tilde{\sigma}_{r\theta}(\pi) = 0, \quad \text{or} \quad \tilde{\phi}(\pi) = 0, \quad \tilde{\phi}_1(\pi) = 0, \end{aligned} \tag{12}$$

and with an imposed symmetry for the case of a tensile crack (pure Mode I)

$$\tilde{\phi}_1(0) = \tilde{\phi}_3(0) = 0. \tag{13}$$

In the case of pure shear (Mode II), we have the boundary conditions in Eqs. (12) as well. We also have to satisfy the following conditions for $\theta = 0$

$$\tilde{\sigma}_{r\theta}(0) = \max \quad \text{and} \quad \tilde{\sigma}_{\theta\theta}(0) = \frac{d\tilde{\sigma}_{r\theta}(0)}{d\theta} = 0 \quad \text{or} \quad \tilde{\phi}(0) = \tilde{\phi}_2(0) = 0. \tag{14}$$

In the mixed mode loading conditions, except for the stress-free boundary conditions (12) and the assumption [4] that the singular parts of strain energy density W must be equal at opposite points on either side of the crack, that is $W(\pi) = W(-\pi)$, it is necessary to introduce additional conditions in intermediate

points of the integration interval from $-\pi$ up to $+\pi$. These conditions have to correspond to the dominant fracture mechanism. It is clear from the preceding discussion that the dominant mechanism (between the two considered) determines the stable crack growth direction. Therefore, we propose to complete the boundary conditions for mixed mode fracture proceeding from the assumption that some dimensionless stress has to have an extremum along the crack growth direction $\theta = \theta^*$.

Then, for fracture mechanism referred to as *tensile crack*, it will be the condition of the crack growth direction along the normal to the maximum tensile stresses, i.e.,

$$\frac{d\tilde{\sigma}_{\theta\theta}(\theta^*)}{d\theta} = 0 \quad \text{or} \quad \tilde{\phi}_1(\theta^*) = 0, \quad -\pi < \theta^* < \pi. \tag{15}$$

This type of boundary condition was proposed in (Dolgorukov [5], Shlyannikov and Dolgorukov [6]). In the case of fracture mechanism referred to as *shear crack*, an additional boundary condition is related to the crack propagation in the direction of maximum shear strains or stresses, i.e.,

$$\frac{d\tilde{\sigma}_{r\theta}(\theta^*)}{d\theta} = 0 \quad \text{or} \quad \tilde{\phi}_2(\theta^*) = 0, \quad -\pi < \theta^* < \pi. \tag{16}$$

In conclusion, the four-order differential Eq. (10) for plane strain and Eq. (11) for plane stress, respectively, are solved numerically for two groups of boundary conditions. Each of them corresponds to the dominating fracture mechanism: the tensile crack [Eqs. (12) and (15)] and the shear crack [Eqs. (12) and (16)].

Method of Solution. For the purpose of solution of nonlinear eigenvalue equations, apply both the shooting method and the finite-difference method. These two methods are applied using iteration. However, the shooting method and its variants were inadequate for mixed mode analysis. A more correct method employing the finite difference procedure was used in our investigation and highly accurate solutions with very rapid convergence were obtained.

The nonlinear fourth-order differential eigenvalue equations (10) and (11) for plane strain and plane stress conditions are solved numerically by means of transformation to the system of first-order differential equations

$$\begin{cases} \dfrac{d\tilde{\phi}}{d\theta} = \tilde{\phi}_1, \\ \dfrac{d\tilde{\phi}_1}{d\theta} = \tilde{\phi}_2, \\ \dfrac{d\tilde{\phi}_2}{d\theta} = \tilde{\phi}_3, \\ \dfrac{d\tilde{\phi}_3}{d\theta} = \varphi(\tilde{\phi}, \tilde{\phi}_1, \tilde{\phi}_2, \tilde{\phi}_3). \end{cases} \tag{17}$$

The finite-difference counterpart for system (17) is introduced as

$$\begin{cases} \widetilde{\phi}_{i+1} - \widetilde{\phi}_i = \dfrac{\Delta\theta_i}{2}(\widetilde{\phi}_{1,i+1} + \widetilde{\phi}_{1,i}), \\ \widetilde{\phi}_{1,i+1} - \widetilde{\phi}_{1,i} = \dfrac{\Delta\theta_i}{2}(\widetilde{\phi}_{2,i+1} + \widetilde{\phi}_{2,i}), \\ \widetilde{\phi}_{2,i+1} - \widetilde{\phi}_{2,i} = \dfrac{\Delta\theta_i}{2}(\widetilde{\phi}_{3,i+1} + \widetilde{\phi}_{3,i}), \\ \widetilde{\phi}_{3,i+1} - \widetilde{\phi}_{3,i} = \dfrac{\Delta\theta_i}{2}(\varphi_{i+1} + \varphi_i) \qquad (i = 1, \ldots, i_{\max}). \end{cases} \tag{18}$$

Here $i_{\max}$ is the number of node points within the interval $-\pi \le \theta \le \pi$. The step size of integration $\Delta\theta_i = \theta_{i+1} - \theta_i$ was varied in an appropriate manner. The solution of the nonlinear equation (17) to transfer to finding of the roots for the algebraic system (18). Before describing the solution of Eqs. (17), we shall formulate the Cauchy problem for the same system. Let us assume an approximate solution for vth iteration to be known. The last equation of system (17) can be treated as one nonlinear equation with respect to variable $\widetilde{\phi}_{3,i+1}^{(v+1)}$ and written in the form

$$\Phi(\widetilde{\phi}_{3,i+1}^{(v+1)}) \equiv \widetilde{\phi}_{3,i+1}^{(v+1)} - \widetilde{\phi}_{3,i} -$$

$$-\{\varphi_{i+1}[\widetilde{\phi}_{i+1}(\widetilde{\phi}_{3,i+1}^{(v+1)}), \widetilde{\phi}_{1,i+1}(\widetilde{\phi}_{3,i+1}^{(v+1)}), \widetilde{\phi}_{2,i+1}(\widetilde{\phi}_{3,i+1}^{(v+1)}), \widetilde{\phi}_{3,i+1}^{(v+1)}] +$$

$$+\varphi_i(\widetilde{\phi}_i, \widetilde{\phi}_{1,i}, \widetilde{\phi}_{2,i}, \widetilde{\phi}_{3,i})\}\frac{\Delta\theta_i}{2} = 0, \tag{19}$$

in which values $\widetilde{\phi}_{i+1}$, $\widetilde{\phi}_{1,i+1}$, and $\widetilde{\phi}_{2,i+1}$ are expressed through first three equations of system (17):

$$\begin{aligned} \widetilde{\phi}_{2,i+1}^{(v+1)} &= \widetilde{\phi}_{2,i} + \frac{\Delta\theta_i}{2}(\widetilde{\phi}_{3,i+1}^{(v+1)} + \widetilde{\phi}_{3,i}), \\ \widetilde{\phi}_{1,i+1}^{(v+1)} &= \widetilde{\phi}_{1,i} + \frac{\Delta\theta_i}{2}\left[2\widetilde{\phi}_{2,i} + \frac{\Delta\theta_i}{2}(\widetilde{\phi}_{3,i+1}^{(v+1)} + \widetilde{\phi}_{3,i})\right], \\ \widetilde{\phi}_{i+1}^{(v+1)} &= \widetilde{\phi}_i + \frac{\Delta\theta_i}{2}\left\{2\widetilde{\phi}_{1,i} + \frac{\Delta\theta_i}{2}\left[2\widetilde{\phi}_{2,i} + \frac{\Delta\theta_i}{2}(\widetilde{\phi}_{3,i+1}^{(v+1)} + \widetilde{\phi}_{3,i})\right]\right\}. \end{aligned} \tag{20}$$

The equation (20) is solved by the Newton method

$$\widetilde{\phi}_{3,i+1}^{(v+1)} = \widetilde{\phi}_{3,i+1}^{(v)} - \frac{\Phi(\widetilde{\phi}^{(v)}, \widetilde{\phi}_1^{(v)}, \widetilde{\phi}_2^{(v)}, \widetilde{\phi}_3^{(v)})}{\partial\Phi^{(v)} / \partial\widetilde{\phi}_{3,i+1}}. \tag{21}$$

The iterations proceed by v until the difference between the consecutive values of $\widetilde{\phi}_{3,i+1}^{(v+1)}$ and $\widetilde{\phi}_{3,i+1}^{(v)}$ is less than a given number

$$\left|\widetilde{\phi}_{3,i+1}^{(v+1)} - \widetilde{\phi}_{3,i+1}^{(v)}\right| < \varepsilon. \tag{22}$$

More details of the solution are described in [7].

Mode Mixity Parameters Determination. For the mixed mode small-scale yielding problem, two parameters K_M^p and M_P introduced by Shih (1974) are required to specify completely the stress and strain fields in the vicinity of the crack tip. As has already been discussed related to Eqs. (7), $K = K_M^p$ is the amplitude of the dominant singularity or plastic stress intensity factor and M_P is the near-field mixity parameter

$$M_P = \frac{2}{\pi}\tan^{-1}\left|\frac{\widetilde{\sigma}_{\theta\theta}(\theta=0)}{\widetilde{\sigma}_{r\theta}(\theta=0)}\right|. \tag{23}$$

As follows from the above method based on the boundary conditions, the angular distribution of stresses and strains depends on the crack growth direction angle θ^* or the dominant fracture mechanism. From our solutions which are given below, we can point out that, for each particular value of θ^*, one or generally two values of M_P ranging from pure Mode I to pure Mode II can be found. Thus, the crack deviation angle θ^* to identify each possible set of dimensionless stresses and strains distributions and M_P cannot be thought of as a unique measure of the near-field in the light of the fracture mechanism under mixed mode loading. In turn, the crack growth direction angle θ^* can be found through any fracture criterion expressed in terms of the elastic stress intensity factors. Several different criteria have been proposed for determining the direction of crack growth under general mixed mode loading conditions (see, for example the criterion by Shlyannikov and Braude [8]). Hence, it is possible to connect the near-field to the far-field which by-passes an analysis of the intermediate field as it was proposed in Part 1 by equation (14). Unlike the investigation of Shih [3], plastic mixity parameter M_P in the present work will directly be obtained from both dimensionless $\widetilde{\sigma}_{\theta\theta}$ and $\widetilde{\sigma}_{r\theta}$ distributions without a finite element analysis of intermediate fields, but calculating the relationship between elastic and plastic mixity parameters.

In accordance with the approach by Shih [3], the plastic stress intensity factor K_M^p in pure Mode I (or pure Mode II) can directly be expressed in terms of corresponding elastic stress intensity factor using Rice's J-integral. In mixed mode small-scale yielding, K_M^p can also be expressed in terms of the J-integral (Shih [3]). That is

$$J = \frac{K_1^2 + K_2^2}{E'} = \frac{\alpha\sigma_0^2}{E'} I_n(\theta^*)(K_M^p)^{n+1} \quad \text{and} \quad K_M^p = \left[\frac{K_1^2 + K_2^2}{\alpha\sigma_0^2 I_n(\theta^*)}\right]^{1/(n+1)}, \quad (24)$$

where K_1 and K_2 are elastic stress intensity factors

$$K_1 = \frac{\sigma\sqrt{\pi a}}{2}[(1+\eta) - (1-\eta)\cos 2\beta] \quad \text{and} \quad K_2 = \frac{\sigma\sqrt{\pi a}}{2}(1-\eta)\sin 2\beta, \quad (25)$$

and $E' = E$ for plane stress, $E' = E/(1-\nu^2)$ for plane strain, where ν is Poisson's ratio.

In the above relations, α and n are the hardening parameters, a is the half crack length, β is the inclined angle of crack to the y-axis, and η is the biaxial normal stress ratio. Different degrees of biaxiality and mixed mode are given by the combinations of β and η. Tensile load corresponds to $\beta = 90°$ for any η, and pure shear load to $\beta = 45°$, $\eta = -1$. Note that the crack growth direction angle is a function of these parameters [i.e., $\theta^* = \theta^*(\sigma, \beta, \eta, \nu, r/a)$] expressed in the form of a fracture criterion.

The numerical constant $I_n(\theta^*)$ is obtained from the singularity analysis by means of conjugation solutions for far- and near-fields

$$\int_{\Gamma_1} (Wdy - \sigma_{ij} n_j u_{i,x} ds) = 0.5\pi(1-\nu^2)\sigma^2[(1+\eta^2) - (1-\eta^2)\cos 2\beta]. \quad (26)$$

After transformation of the left part of Eq. (26), we have the following expression for the integral along contour Γ_2 close to crack tip

$$\int_{\Gamma_2} (Wdy - \sigma_{ij} n_j u_{i,x} ds) = \alpha_0 (K_M^p)^{n+1} r^{(n+1)(s-2)+1} I_n(\theta^*), \quad (27)$$

where

$$I_n(\theta^*) = \int_{-\pi}^{\pi} \Omega(n,\theta) d\theta, \quad (28)$$

and

$$\Omega = \frac{n}{n+1}\tilde{\sigma}_e^{n+1}\cos\theta - \left[\tilde{\sigma}_{rr}\left(\tilde{u}_\theta - \frac{d\tilde{u}_r}{d\theta}\right) - \tilde{\sigma}_{r\theta}\left(\tilde{u}_r - \frac{d\tilde{u}_\theta}{d\theta}\right)\right]\sin\theta -$$

$$-\frac{1}{n+1}(\tilde{\sigma}_{rr}\tilde{u}_r + \tilde{\sigma}_{r\theta}\tilde{u}_\theta)\cos\theta.$$

Employing the Ramberg–Osgood relation between stresses and strains and the stress components derived from the stress function Airy as well, we can obtain the dimensionless radial and tangential displacements for *plane strain* and their derivatives included in the previous equation

$$\tilde{u}_r(\theta)=\frac{3}{4}(n+1)\tilde{\sigma}_e^{n-1}[a_2\tilde{\phi}+\tilde{\phi}_2],\quad \tilde{u}_\theta(\theta)=\frac{n+1}{n}\left[\frac{d\tilde{u}_r}{d\theta}-3\tilde{\sigma}_e^{n-1}(1-s)\tilde{\phi}_1\right], \quad (29)$$

where

$$\frac{d\tilde{u}_r}{d\theta}=\frac{3(n+1)}{4}\tilde{\sigma}_e^{n-3}\left[\frac{n-1}{2}\varphi_1(a_2\tilde{\phi}+\tilde{\phi}_2)+\tilde{\sigma}_e^2(a_2\tilde{\phi}_1+\tilde{\phi}_3)\right],$$

$$\varphi_1=\frac{3}{2}(a_2\tilde{\phi}+\tilde{\phi}_2)(a_2\tilde{\phi}_1+\tilde{\phi}_3)+2a_4\tilde{\phi}_1\tilde{\phi}_2,$$

$$\tilde{u}_\theta-\frac{d\tilde{u}_r}{d\theta}=\frac{1}{n}\frac{d\tilde{u}_r}{d\theta}-3\frac{n+1}{n}\tilde{\sigma}_e^{n-1}(1-s)\tilde{\phi}_1,\qquad \tilde{u}_r+\frac{d\tilde{u}_\theta}{d\theta}=(s-2)\tilde{u}_r,$$

while the following expressions hold for *plane stress*

$$\begin{aligned}\tilde{u}_r(\theta)&=\frac{1}{n(s-2)+1}\tilde{\sigma}_e^{n-1}\left\{s(3-s)\frac{\tilde{\phi}}{2}+\frac{d^2\tilde{\phi}}{d\theta^2}\right\},\\ \tilde{u}_\theta(\theta)&=\frac{n+1}{n}\left[\frac{d\tilde{u}_r(\theta)}{d\theta}-3\tilde{\sigma}_e^{n-1}(1-s)\frac{d\tilde{\phi}(\theta)}{d\theta}\right],\end{aligned} \quad (30)$$

where

$$\frac{d\tilde{u}_r(\theta)}{d\theta}=\frac{\tilde{\sigma}_e^{n-1}}{n(s-2)+1}\left\{\frac{(n-1)\psi_1}{2\tilde{\sigma}_e^2}\left[\frac{s(3-s)}{2}\tilde{\phi}+\frac{d^2\tilde{\phi}}{d\theta^2}\right]+\frac{s(3-s)}{2}\frac{d\tilde{\phi}}{d\theta}+\frac{d^3\tilde{\phi}}{d\theta^3}\right\},$$

$$\frac{d\tilde{u}_\theta(\theta)}{d\theta}=\tilde{\sigma}_e^{n-1}\left[s\left(s-\frac{3}{2}\right)\tilde{\phi}-\frac{1}{2}\frac{d^2\tilde{\phi}}{d\theta^2}\right]-\tilde{u}_r(\theta),$$

$$\psi_1=2s^2(s^2-3s+3)\tilde{\phi}\frac{d\tilde{\phi}}{d\theta}+(5s^2-9s+6)\frac{d\tilde{\phi}}{d\theta}\frac{d^2\tilde{\phi}}{d\theta^2}+$$

$$+2\frac{d^2\tilde{\phi}}{d\theta^2}\frac{d^3\tilde{\phi}}{d\theta^3}+s(3-s)\tilde{\phi}\frac{d^3\tilde{\phi}}{d\theta^3}.$$

It should be noted that the integration constant given by Eq. (28) has different values under plane stress and plane strain which are denoted as I_n^{2D} and I_n^{3D}, respectively. The amplitude K_M^p has been introduced since it is convenient to normalize the dimensionless stress tensor $\tilde{\sigma}_{ij}(\theta,n,M_P)$ so that effective stress $[\tilde{\sigma}_e(\theta,n,M_P)]$ is equal to 1. Thus, for small-scale yielding, that is when the plastic zone near the crack tip is very small compared to crack length, the amplitude of the singularity K_M^p can directly be determined by application of the J-integral [Eq. (24)].

Finally, the nonlinear governing equations (10) and (11) for both types of the dominating fracture mechanisms can be solved numerically using the iteration scheme with error and step-size control. Due to the mixed mode loading, we need to consider the crack-tip fields from $\theta = -\pi$ to $\theta = +\pi$. To satisfy the stress-free boundary conditions, we have $\tilde{\sigma}_{\theta\theta} = \tilde{\sigma}_{r\theta} = 0$ at $\theta = \pm\pi$. We also reinforce the boundary conditions that are related to the leading fracture mechanism so that the stresses $\sigma_{\theta\theta}$ and $\sigma_{r\theta}$ are extrema along the crack growth direction $\theta = \theta^*$.

Results and Discussion. In this section, we study the general mixed mode loading conditions. For the cases that we consider here, we introduce two types of crack-tip fields. The first one, referred to as tensile crack field type, corresponds to Mode I predominant loading conditions [Eqs. (12), (15)]. The other, shear crack field type, is related to Mode II predominant loading conditions [Eqs. (12), (16)]. One of such boundary conditions is set at points $\theta = \theta^*$ predetermining the crack growth direction. Thus, the variable $\theta = \theta^*$ possesses consecutive values in a range from $\theta^* = 0$ up to $\theta^* = -80°$ with step size equal to 5°. It should be noted that we have pure Mode I at $\theta^* = 0$ for the tensile crack, while pure Mode II takes place for the shear crack. For each value of $\theta = \theta^*$, with the help of the obtained dimensionless stress distributions, the appropriate values of plastic mixity parameter M_P are calculated that identify each concrete case of the mixed mode crack behavior.

Besides, in our numerical computations with predominant Mode I loading conditions, the mixity parameter M_P varies from 1 to 0 by varying $\theta = \theta^*$ from $\theta^* = 0$ up to $\theta^* = -(70 - 80°)$, respectively, depending on the strain-hardening exponent n.

In the case of predominant Mode II fracture mechanism, M_P changes from 0 (at $\theta^* = 0$) to 1. Our analysis and computation data for the two-dimensional problem take into account the different crack behavior for two main types of stress-strain state because the results for plane strain and plane stress are contrasted.

According to our numerical results, the angular variations of the dimensionless singular crack-tip stress and strain fields, $\tilde{\sigma}_{\theta\theta}$ and $\tilde{\varepsilon}_{r\theta}$, are shown in Fig. 2a–d for the two materials corresponding to the strain-hardening exponent $n = 3$ and $n = 13$, respectively.

Note that when we construct the power-law solutions, we assume that the extrema of the singular stresses $\tilde{\sigma}_{\theta\theta}$ and $\tilde{\sigma}_{r\theta}$ (or $\tilde{\varepsilon}_{r\theta}$) corresponding to the dominant fracture mechanisms exist in the crack growth direction $\theta = \theta^*$. This fact is confirmed in Fig. 2, where the angular variations of $\tilde{\sigma}_{\theta\theta}$ and $\tilde{\varepsilon}_{r\theta}$ are shown for various values $\theta = \theta^*$ (and consequently for different values of the mixity parameter M_P). The crack-tip fields shown in Fig. 2a, b are the tensile crack type fields while in Fig. 2c, d are presented the shear crack type fields. These results are necessary to establish dependence between θ^* and M_P for each of the considered dominant fracture mechanisms. From Fig. 2a, b, it is clear that the departure from Mode I conditions (that is, M_P less than unity) gives rise

to a reduction in the peak value of the amplitude of the tensile stress component $\widetilde{\sigma}_{\theta\theta}$ associated with the tensile crack dominant singularity in the plastic zone of the crack-tip. Distributions similar to those shown in Fig. 1 have been determined for $n = 2, 3, 5, 9$, and 13 and plane stress conditions.

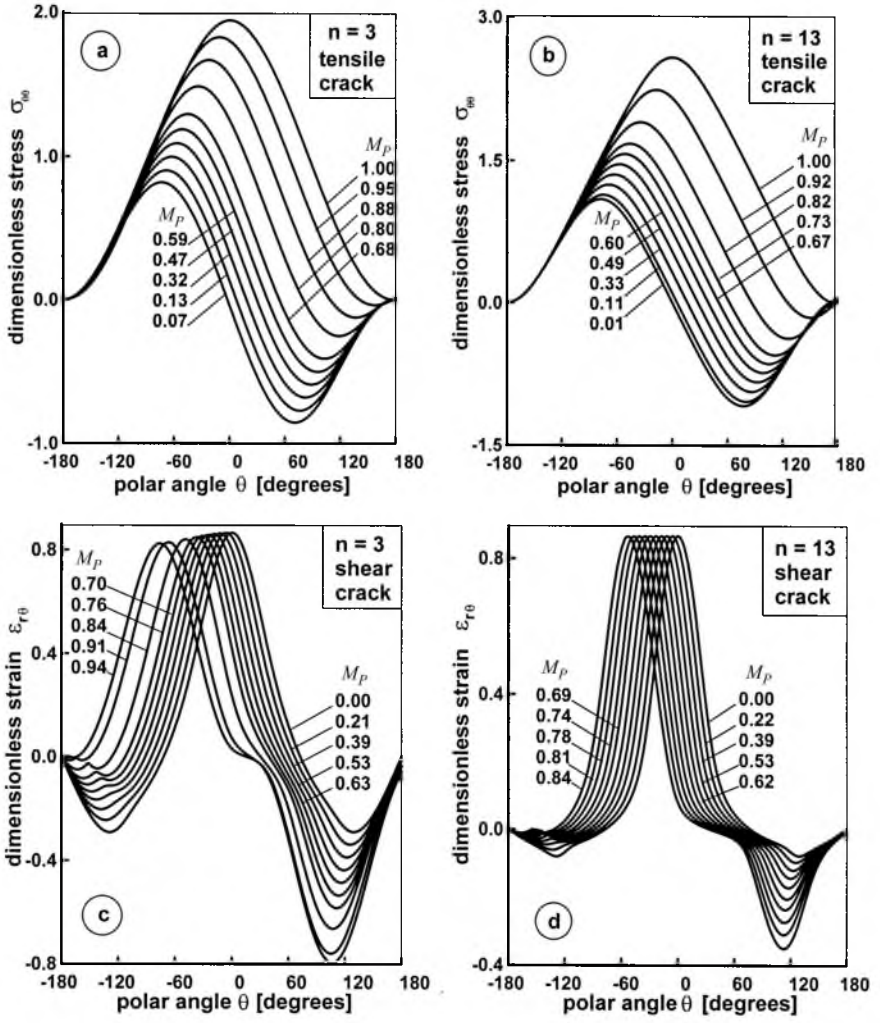

Fig. 2. Angular variations of (a, b) tensile stresses and (c, d) shear strains for different near-tip mixities corresponding to $n = 3$ and $n = 13$ under plane strain.

Summarized Mixed Mode Crack Behavior Parameters. The maximum tensile stress and maximum shear stress (or strain) criteria have been used in experimental studies of the crack growth direction in mixed mode fracture for brittle and ductile materials [8–10]. Some experimental results show that the angle of crack growth direction coincides with the maximum tensile stress position. On the other hand, high Mode II components induced shear-controlled failure. Predominant Mode II loading drives the crack in the maximum shear direction. In ductile steels, in pure Mode II conditions, the stable crack extends approximately in its original direction (that is, $\theta^* \approx 0$). The predicted directions

of maximum tensile stress and maximum shear according to our small-scale yielding plane-strain analysis (for example, results in Fig. 2 and others) for the work-hardening materials with $n = 2, 3, 5, 9$, and 13 are summarized in Fig. 3a. The upper set of curves is related to the tensile crack fracture mechanism and agree with [3], whereas the lower set curves correspond to the shear crack fracture mechanism.

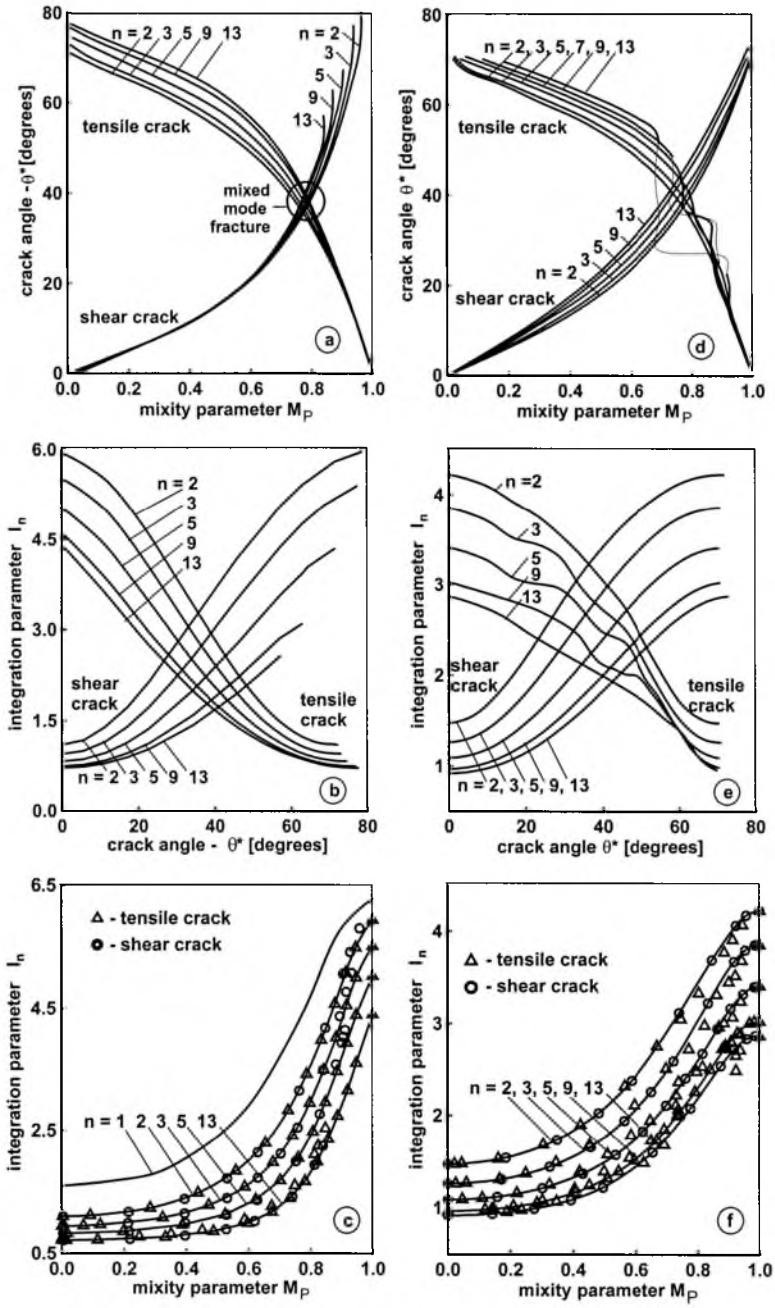

Fig. 3. Integration parameter I_n and crack angle θ^* as functions of the near-tip mode-mixity M_P and strain-hardening exponent, (a, b, c) – plane strain, (d, e, f) – plane stress.

Similar results under plane stress conditions are shown in Fig. 3d. Unlike the plane strain conditions, under the plane stress despite the presence of some discontinuity areas on the upper crack surface, the trend to achieve the maximal magnitude of the tensile stress for $M_P \in (0.65 - 0.90)$ is clear. This is connected with omitting the elastic terms in a complementary potential energy functional. As can be seen, this uncertain behavior area comes into existence at $n > 5$ and its size increases as the strain-hardening exponent value increases. Note that the behavior of the shear crack under plane stress is more sensitive to the variation of the strain-hardening coefficient than under plane-strain conditions.

The method developed by Li [11] allows a simple evaluation of the plastic mixity parameter without analysis of the near tip field by decomposing the I_n-integral into symmetrical and anti-symmetrical parts with respect to the crack axis. By considering these decompositions, two sets of the integral parameters $I_n^{*\mathrm{I}}$ and $I_n^{*\mathrm{II}}$ were obtained which are functions of the power hardening coefficient n and mixity parameter M_P. Here I_n is the corresponding integration constant defined in [3] and by the proposed Eq. (28). However, as was mentioned earlier, M_P is not univocal parameter that is necessary for identification of the near-tip asymptotic fields. In contrast to this, the integration constant I_n obtained from Eq. (28) through the crack growth direction angle θ^* is a strong function of the dominant fracture mechanism as is shown in Fig. 3b and 3e for plane strain and plane stress, respectively. Moreover, I_n is an essential parameter allowing the determination of the plastic stress intensity factor by Eq. (24). According to our approach, the relationship between the plastic mixity parameter M_P and the integration constant I_n is established for both the dominant fracture mechanisms and shown in Fig. 3c and 3f in plane strain and plane stress, respectively, for different hardening coefficient n. It can be seen that Fig. 3c is in good agreement with the Shih's data [3] who carried out an intermediate field analysis by the finite element calculations to obtain the $M_P - M_E$ relationship for small-scale yielding. The principal advantage of our approach is that the mixity parameter M_P can be evaluated immediately from the stress field solution by Eqs. (10) and (11) taking into account Eqs. (12)–(16) with any types of the boundary conditions. The results of the present work plotted in Fig. 3c and 3f support the argument that K_M^p is the general plastic stress intensity factor (instead of the elastic K_1 and K_2) in mixed-mode small-scale yielding conditions even though there are two different type of the dominant fracture mechanism.

In order to determine whether both the maximum tensile stress and the maximum shear stress crack propagation direction criteria are appropriate to directly connect the near-field to the far-field, the scheme of [(14), Part 1] is applied. Following the scheme (14), by using the M_E versus θ^* curves of Fig. 4 (Part 1) as well as the θ^* versus M_P curves of Fig. 3a, d, M_P can be translated into a function of M_E for small-scale yielding as shown in Fig. 4, for instance, under equibiaxial tension–compression ($\eta = -1$). The plots clearly show that the computed values of M_P for a given M_E for the tensile crack differed from the results for the shear crack for the same stressed state and the same value of n. It is

concluded that the relation of M_P to M_E depends primarily on the crack growth direction criterion and the non-singular term and secondary on the strain-hardening exponent n. It is not surprising that the strain-hardening behaviour exhibited in the shear crack case, where the plastic strain is less constrained, could be different from that exhibited in the tensile crack case. The computed range of $M_P - M_E$-variation under plane strain calculated by scheme (14) coincides, in general, with finite element study of Shih [3], however, our approach permits the clear identification of the nominal biaxial stress state with respect to parameter governing plastic mixed-mode crack behavior.

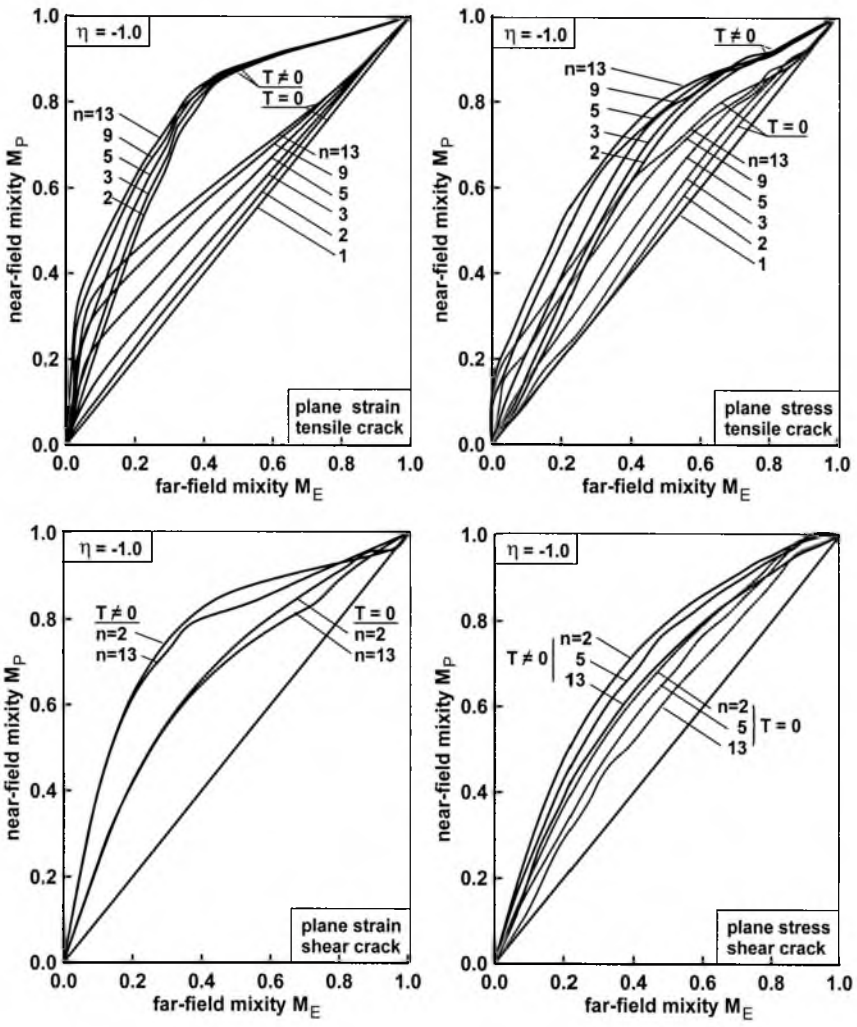

Fig. 4. Near-field mixity M_P versus far-field mixity M_E by the maximum tensile (tensile crack) and shear stress (shear crack) criteria for equibiaxial tension–compression ($\eta = -1$).

In Fig. 5 are shown dependencies between $M_P - M_E$ according to both considered criteria for the compact-tension-shear specimen developed by Richard and Benitz [12] which allows to realize in a full range of mixed mode loadings from the pure Mode I to pure Mode II.

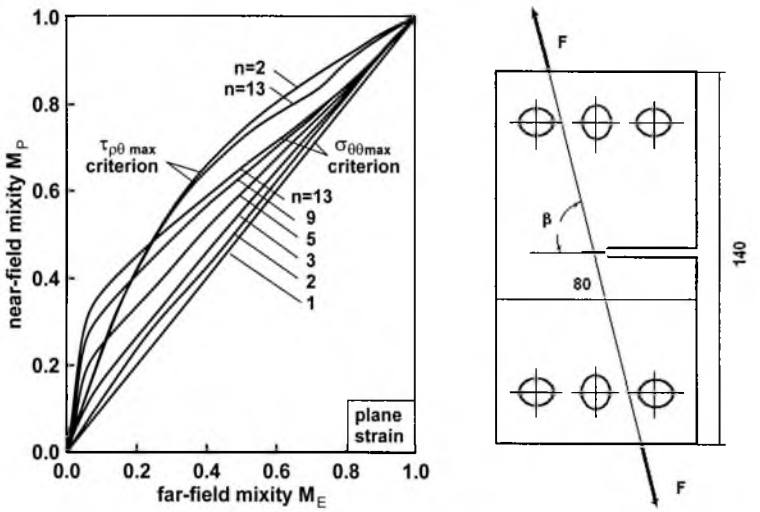

Fig. 5. Near-field mixity M_P versus far-field mixity M_E for compact-tension-shear specimen.

Some experimental results [9, 10, 13] give a rough empirical estimate of the critical applied mixed mode ratio characterizing the usual change in fracture mode. As follows from these experimental data, which are shown in Fig. 6 for various ferritic steels, the transition of the fracture mode occurs at a relatively constant elastic mixity parameter M_E value of 0.68. In mixed mode loading, this M_E-value corresponds to the plastic mixity parameter, approximately $M_P \approx 0.75 - 0.85$ depending on the strain-hardening exponent n. These experimental results are exactly confirmed by our numerical data that are represented for plane strain in Fig. 3a. It is clear that the crossing area of separate curves, corresponding to each (between two considered) dominating mechanism, form a small zone of the truly mixed mode fracture. The position of this zone of unstable equilibrium corresponds to the change of the leading fracture mechanism. As is shown in Fig. 3a, the mixed transition angle ($\theta^* \approx 35 - 45°$) could be influenced also by the strain-hardening exponent.

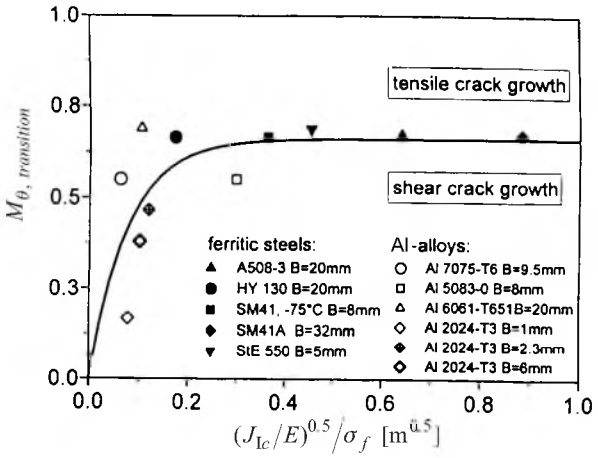

Fig. 6. Mixed mode ratios M_E characterizing the change in fracture mode (reproduced from [9]).

Another complicating background of our analytical results can be found by comparison with experimental data [14] related to the Stage I–Stage II transition under low cycle fatigue failure. They have used the expression of Tanaka [15] for effective elastic stress intensity factor, K_{eff}, to find the fastest mode on crack growth, Stage I or Stage II under biaxial loading with an applied normal stress σ_a, and a shear stress τ. Solution [14] gives a condition for the state of stress at the Stage I–Stage II transition, i.e., $\mu = 4\tau^2/\sigma_a^2 = 1.077$, when the shear to tensile strain ratio for plastic fracture is $\lambda = 1.56$ while for elastic crack behavior $\lambda = 1.35$. Making use of the expressions [14] for stress intensity factors, giving Mode I and Mode II crack opening

$$K_1 = (\sigma_a/2)\sqrt{\pi a} \qquad \text{and} \qquad K_2 = (\sqrt{(\sigma_a/2)^2 + \tau^2})\sqrt{\pi a}, \tag{31}$$

we may obtain the elastic mixed mode parameter as follows

$$M_E = \frac{2}{\pi}\tan^{-1}\left|\frac{K_1}{K_2}\right| = \frac{2}{\pi}\tan^{-1}\left|\sqrt{\frac{(\sigma_a/2)^2}{(\sigma_a/2)^2 + \tau^2}}\right| = \frac{2}{\pi}\tan^{-1}\left|\frac{1}{\sqrt{1+\mu}}\right|. \tag{32}$$

Substituting $\mu = 1.077$ into previous equation, one obtains $M_E = 0.611$. Thus, although our analysis is only applicable to small-scale yielding around crack tips, the theoretical transition values $M_E = 0.60$–0.75 for plane strain agree surprisingly well with experimental values for structural steels with different properties of [14], $M_E = 0.61$, and [9], $M_E = 0.68$. Authors [14] consider that the cause of the Stage I–Stage II transition has been associated with microstructural features such as grain boundaries and also with the stress-strain state and the strain amplitude because higher ranges making a transition more likely. As the tensile strain component was increased, reducing λ, Stage II cracks appeared, becoming dominant in fatigue fracture.

As is seen in Fig. 6 the transient area for aluminum alloys takes range on M_E from 0.25 to 0.75. Note that the specimen thickness for both the ferritic steels and the aluminum alloy Al6061-T651 is 5–32 mm that assumes the realization of the plane strain conditions under tests. In contrast, for aluminum material Al2024-T3 the thickness is 1–6 mm that corresponds to the plane stress state. These experimental results for aluminum alloy Al2024-T3 agree well with our analytical predictions indicating for the plane stress the range of the dominant fracture mechanism change on M_P as 0.5–0.95.

Conclusions. Unlike the well-known approach of Shih to calculate the relationship between M_E and M_P, in the present paper, the near-field mixity parameter M_P was obtained directly from the compatibility equation with accordance to proposed new scheme of the solution [by the Part 1 through the equation (14)]. The results of both numerical and analytical investigations given in the present work demonstrate that mode mixity parameters as M_E, M_P, and I_n are sensitive to the crack growth direction criteria. One of the main results is also the establishment of the distinction in the crack behavior under the plane strain and the plane stress. Besides the qualitative characteristics corresponding to

each fracture mechanism in the whole range of the mixed mode loading such as the constant of integration I_n are found. This will enable us to use the $I_n - \theta^*$ locus and the $\theta^* - M_P$ locus, a more reasonable approach in the physical sense, rather than the presently used $I_n - M_P$ locus as fracture criteria in the elastic-plastic mixed mode fracture investigations. The present solutions suggest that outside the transition zone dominates only one leading fracture mechanism: either the tensile crack or the shear crack. Strictly speaking, the presence of traces of another fracture mechanism almost always is found on the fracture surface, therefore we should speak about the domination of a mechanism, but not of its certain existence.

Acknowledgements. Funding for this study was provided by the Russian Foundation for Basic Researches through grant 03-01-96233 and the Foundation of Academy of Sciences of Tatarstan Republic through grant 05-5.3-218/2003(f).

Резюме

Запропоновано новий підхід до розв'язання задач змішаних видів руйнування, що базується на деформаційній теорії пластичності зі степеневим зміцненням та використанні пружного і пластичного параметрів змішаності. У залежності від умов змішаності навантаження і вихідного направлення лінії тріщини цей підхід дозволяє оцінити широкий спектр можливих траєкторій розповсюдження тріщини: за механізмами зсуву і відриву. Для двовимірної задачі в полярній системі координат використовується рівняння рівноваги з функцією Ері, для матеріалу зі степеневим зміцненням – модель Рамберга–Осгуда. За допомогою методу скінченних різниць отримано числовий розв'язок задачі змішаності навантаження для граничних умов, що відповідають двом випадкам розповсюдження тріщини. На основі запропонованого підходу визначено залежності параметрів змішаності від різних параметрів навантаження та нахилу тріщини за різних значень показника зміцнення, що добре узгоджуються з експериментальними даними.

1. J. W. Hutchinson, "Singular behavior at the end of a tensile crack in a hardening material," *J. Mech. Phys. Solids*, **16**, 13–31 (1968).
2. J. R. Rice and G. F. Rosengren, "Plane strain deformation near a crack tip in power law hardening material," *Ibid.*, 1–12 (1968).
3. C. F. Shih, "Small-scale yielding analysis of mixed plane strain crack problem," in: *Fracture Analysis*, ASTM STP 560, Philadelphia (1974), pp. 187–210.
4. B. Budiansky and J. R. Rice, "Conservations laws and energy-release rates," *J. Appl. Mech.*, **3**, 201–203 (1973).
5. V. A. Dolgorukov, "Elastic-plastic problem for determination of singular stress-strain-state at inclined crack tip under plane stress conditions," in: *VINITI 4340-V88* (1988), pp. 1–21.
6. V. N. Shlyannikov and V. A. Dolgorukov, "Analysis of the crack propagation under biaxial cyclic load taking into account their orientation," in: Proc. 7th European Conference on Fracture, Budapest (1988), **2**, pp. 1095–1103.

7. V. N. Shlyannikov, *Elastic-Plastic Mixed Mode Fracture Criteria and Parameters*, Springer, Berlin (2003).
8. V. N. Shlyannikov and N. Z. Braude, "A model for predicting crack growth rate for mixed mode fracture under biaxial loads," *Fatigue Fract. Eng. Mater. Struct.*, **15**, 825–844 (1992).
9. C. Dalle Donne, "The crack tip displacement vector approach to mixed-mode fracture," in: *Mixed-Mode Crack Behavior*, ASTM STP1359, Philadelphia (1999), pp. 21–40.
10. Y.-J. Chao and X.-K. Zhu, "A simple theory for describing the transition between tensile and shear mechanisms in mode I, II, III, and mixed mode fracture," in: *Mixed-Mode Crack Behavior*, ASTM STP1359, Philadelphia (1999), pp. 41–57.
11. J. Li, "Estimation of the mixity parameter of a plane strain elastic-plastic crack by using the associated *J*-integral," *Eng. Fract. Mech.*, **61**, 355–368 (1998).
12. H. A. Richard and K. Benitz, "A loading device for creation of mixed mode in fracture mechanics," *Int. J. Fract.*, **22**, 55 (1983).
13. D. Bhattacharjee and J. F. Knott, "Ductile fracture in HY100 steel under mixed mode I mode II loading," *Acta Metall. Mater.*, **42**, 1747–1754 (1994).
14. M. W. Brown and K. J. Miller, "Initiation and growth of cracks in biaxial fatigue," *Fatigue Fract. Eng. Mater. Struct.*, **1**, 231–246 (1979).
15. K. Tanaka, "Fatigue crack propagation from a crack inclined to the cyclic tensile axis," *Eng. Fract. Mech.*, **6**, 493–507 (1974).

Received 31. 10. 2004